

# 光学学报

## 用于静态/动态复合信号的改进对称解调技术

贾景善\*

西安科技大学通信与信息工程学院, 陕西 西安 710054

**摘要** 提出一种可测量外腔式 Fabry-Perot 传感器所加载的静态/动态复合信号的腔长自补偿改进对称解调技术。在对称解调技术的基础上, 通过其输出信号的直流量判断传感器腔长的变化, 从而划分腔长稳定段与突变段, 分段并重新进行信号解调, 以保证动态分量的解调精度; 同时利用腔长变化前后计算出的干涉信号相位差对腔长的变化量进行补偿, 以提高静态分量的测量精度。实验证明该解调技术能够实现对静态/动态复合信号的测量。实验中实现了幅度超过  $100 \mu\text{m}$  复合信号的解调, 大幅度腔长变化量的测量误差约为 2%。该解调技术能够解调不同腔长传感器上加载的包含高频分量的静态/动态复合信号。

**关键词** 光纤光学; 光纤传感技术; 激光干涉测量; 相位解调; 外腔式 Fabry-Perot 干涉仪

中图分类号 TN253 文献标志码 A

DOI: 10.3788/AOS231309

### 1 引言

光纤传感器具有抗电磁干扰、耐腐蚀、耐高温、高灵敏度等优势, 因此受到广泛关注<sup>[1]</sup>。特别是外腔式 Fabry-Perot 干涉仪 (EFPI) 传感器, 其结构紧凑、抗干扰能力强, 在航空航天、能源化工、生物医疗、安防等领域得到广泛应用<sup>[1-5]</sup>。因此, 应用于这些传感器的解调技术也受到了广泛的研究<sup>[6-16]</sup>。在很多场合下, 待测信号往往是由静态信号和动态信号相叠加而成的复合信号。但是, 对于光纤传感技术, 常用于动态信号测量的激光干涉测量技术<sup>[7-11]</sup>和用于静态信号测量的白光干涉测量技术<sup>[12-15]</sup>存在明显的差别, 激光干涉测量技术要求光源波长保持稳定, 白光干涉测量技术则通过扫描光源获取传感器光谱, 进而实现测量。这导致已有的多参量传感器或测量技术只能用来同时测量不同的静态量<sup>[17-18]</sup>或者不同的动态量<sup>[8]</sup>, 而无法实现静态/动态复合信号的测量, 或者测量系统中使用多个传感器, 通过分时复用实现对不同信号的测量<sup>[19]</sup>。

EFPI 传感器有望通过高速白光干涉测量技术<sup>[14, 16]</sup>实现对静态/动态复合信号的测量。但是, 这类技术往往依赖于高速光谱仪来实现<sup>[14]</sup>, 其解调速率受限于扫描器件, 依然无法满足高频分量的测量要求, 且成本较高; EFPI 传感器依赖于高速扫描的光源实现<sup>[16]</sup>, 而这类光源的带宽较窄, 测量范围受限, 同时, 这类技术的运算量较大, 有时需要线下执行信号的处理过程<sup>[16]</sup>。

多种激光干涉测量技术已经被提出以实现 EFPI 传感器动态信号的解调。由于传感器腔长和激光波长必须严格匹配才能获得正交信号<sup>[9-11, 20-21]</sup>, 因此对于这些解调技术, 如果 EFPI 的腔长明显改变, 则无法恢复出待测信号。Ren 等<sup>[22]</sup>提出利用腔长变化对初始腔长进行补偿的方法, 以提高腔长变化后信号的解调精度。但是, 由于腔长补偿精度不足, 如果腔长变化大于  $40 \mu\text{m}$ , 解调信号将失真<sup>[22]</sup>。2020 年, Jia 等<sup>[23]</sup>提出了用于 EFPI 传感器信号解调的对称解调技术, 该技术无须使传感器腔长和激光波长匹配, 也无须将腔长作为预设参数, 适用于腔长难以确定或波动较大的场合。但是, 该技术在单次测量的过程中将干涉信号间的相位差作为常量来处理, 单次测量中腔长的明显改变会导致测量失败, 其可解调的信号动态范围也限制在十几  $\mu\text{m}$ 。

本文提出了一种用于静态/动态复合信号解调的改进对称解调技术。在对称解调技术的基础上, 通过输出信号的直流量判断传感器腔长的变化, 从而划分腔长稳定段与突变段, 并通过分段后重新进行信号解调, 保证动态分量的解调精度; 同时利用腔长变化前后计算出的干涉信号相位差对腔长的变化量进行补偿, 提高静态分量的测量精度。该技术在腔长大幅度变化的情况下也能够正常执行, 能够实现对静态/动态复合信号的测量。而且该技术属于无源解调技术, 其解调频率的上限只受限于所使用的光电二极管、采集卡等电子器件的性能。该解调技术具有系统简单、稳定、低

收稿日期: 2023-07-26; 修回日期: 2023-09-11; 录用日期: 2023-09-28; 网络首发日期: 2023-10-08

基金项目: 国家自然科学基金青年科学基金(62305265)、陕西省自然科学基础研究计划(2022JQ-613)

通信作者: \*xkjs@xust.edu.cn

成本、应用范围广等优势,具有较好的应用前景。

## 2 解调原理

用于静态/动态复合信号解调的改进对称解调技术测量系统如图1所示。使用三个不同波长的激光器产生三束激光,其波长分别为 $\lambda_1=1546.914\text{ nm}$ 、 $\lambda_2=1550.131\text{ nm}$ 及 $\lambda_3=1553.362\text{ nm}$ ,光功率为10 mW。三路激光通过一个光纤耦合器组进行合束,之后经过一个光隔离器和一个 $2\times 2$ 耦合器注入传感器中。从传感器反射的携带待测信号的光束再次经过耦合器后由波分复用器(WDM)分束。该WDM的工作波长为 $(1546.92\pm 0.11)\text{ nm}$ 、 $(1550.12\pm 0.11)\text{ nm}$ 和 $(1553.33\pm 0.11)\text{ nm}$ ,相邻通道间的隔离度大于30 dB。不同波长的干涉信号经过光电二极管(PD)转换为电信号,之后由采集卡(ADC)采集,ADC的最高采样频率为每通道200 kHz。最终使用计算机完成信号解调。

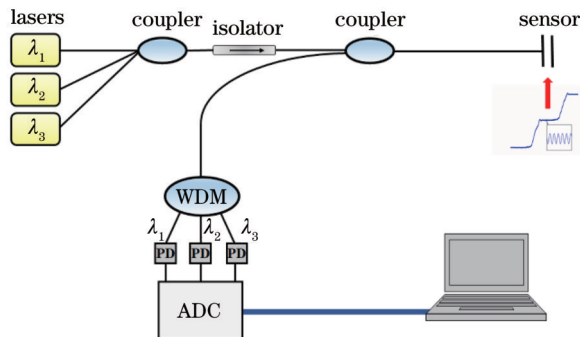


图1 改进对称解调技术系统硬件示意图

Fig. 1 Hardware diagram of improved symmetric demodulation technology system

三路干涉信号可表示为

$$f_i = A + B \cos \left[ \frac{4n\pi}{\lambda_i} (d_0 + d_\Delta) \right], \quad (1)$$

式中: $A$ 为干涉条纹的直流分量; $B$ 为干涉条纹的对比度; $n$ 为EFPI腔内介质的折射率,通常为1; $d_0$ 为传感器的初始腔长; $d_\Delta$ 为腔长受待测信号的影响而产生的变化量; $i=1,2,3$ 。由对称解调技术的波长选取原则<sup>[23]</sup>可知,这三路干涉信号间的相位差相等,则式(1)可表示为

$$f_i = A + B \cos [\theta + (i-2)\delta], \quad (2)$$

其中,

$$\theta = 4n\pi(d_0 + d_\Delta)/\lambda_2, \quad (3)$$

$$\delta = 4n\pi(d_0 + d_\Delta) \left( \frac{1}{\lambda_j} - \frac{1}{\lambda_{j-1}} \right), \quad j=2,3, \quad (4)$$

之后,通过对称解调技术即可得到初次解调的信号<sup>[23]</sup>,令

$$F_1 = f_2 - \frac{f_1 + f_3}{2} = B(1 - \cos \delta) \cos \theta, \quad (5)$$

$$F_2 = \frac{f_1 - f_3}{2} = B \sin \delta \sin \theta, \quad (6)$$

令信号 $F_1$ 的幅值为 $A_F$ ,信号 $F_2$ 的幅值为 $A_f$ ,则 $A_F = kB(1 - \cos \delta)$ , $A_f = kB$ ,其中 $k$ 为 $\cos \theta$ 幅度的峰峰值, $0 < k \leq 2$ 。则有

$$C = \frac{A_F}{A_f} = 1 - \cos \delta, \quad (7)$$

$$E = \sin \delta = \pm \sqrt{1 - \cos^2 \delta}, \quad (8)$$

$E$ 的正负可以通过腔长所处的大致范围确定,则

$$\tan \theta = \frac{CF_2}{EF_1}, \quad (9)$$

$$\theta = \arctan \frac{CF_2}{EF_1}. \quad (10)$$

反正切运算的值域为 $-\pi/2 \sim \pi/2$ ,因此经过相位展开后才能得到完整的相位信号,之后有

$$d_\Delta = \frac{\lambda_2}{4n\pi} \theta. \quad (11)$$

对于大多数无源激光干涉解调技术,在测量过程中将信号间相位差作为已知量<sup>[9-11]</sup>或固定量<sup>[23]</sup>来使用,由此要求 $d_0 \gg d_\Delta$ ,腔长存在明显的变化时会导致解调失效。因此,本解调技术在腔长变化后重新获取相位差,消除腔长变化对待测信号解调的影响;同时,通过式(4)利用相位差的变化量得到腔长的变化量,实现对解调信号直流量的补偿,最终实现对静态/动态复合信号的解调。

如图2所示,复合信号解调的完整过程为:1)通过式(11)得到初步的解调信号 $d_f$ ;2)通过 $d_f$ 分割测量期间腔长的稳定段与突变段;3)分别计算腔长稳定时的相位差 $\delta$ ;4)利用腔长突变段前后的相位差 $\delta$ 均值作为突变段的相位差,重新解调该段信号,通过式(4)反推相邻稳定段的腔长差,对腔长变化量进行校准;5)重新解调各稳定段的待测信号,并将其与校准后的突变段

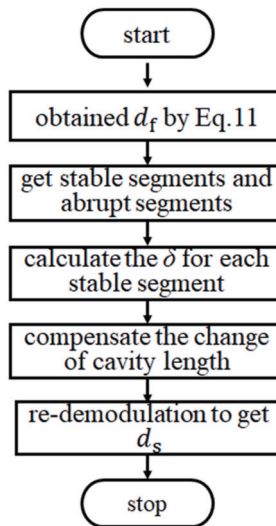


图2 改进对称解调技术的信号解调流程图

Fig. 2 Flowchart of signal demodulation of improved symmetric demodulation technique

解调信号合成为完整的输出信号  $d_s$ 。

### 3 仿真分析

通过将本文改进对称解调技术与对称解调技术<sup>[23]</sup>进行对比,研究了腔长大幅度变化对解调结果的影响。设置光源波长为  $\lambda_1=1546.914\text{ nm}$ 、 $\lambda_2=1550.131\text{ nm}$  及  $\lambda_3=1553.362\text{ nm}$ ,采样频率为 200 kHz,输入信号的动态分量频率为 2 kHz,幅度(峰峰值)为 1.6  $\mu\text{m}$ ,干涉条纹的直流分量 A 及对比度 B 设置为 2 V,初始腔长  $d_0$  为 220  $\mu\text{m}$ 。在 0.055 s 附近,腔长突变了 70  $\mu\text{m}$ ,形成了一个静态/动态复合信号。输入信号如图 3 中信号 input 所示。分别使用对称解调技术、改进对称解调技术进行信号解调,解调信号分别如图 3 中信号 sym 和 c-sym 所示。

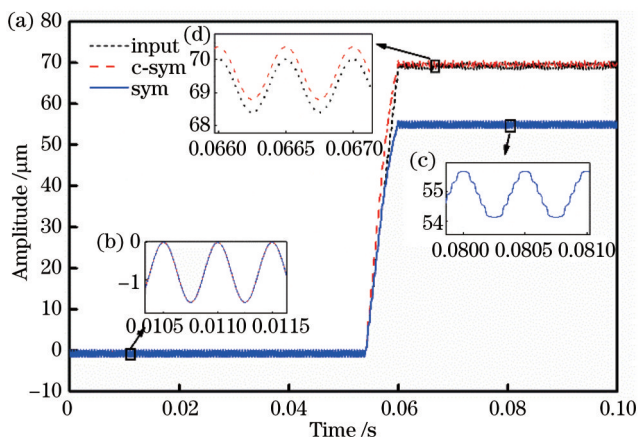


图 3 静态/动态复合信号解调的仿真结果。(a) 输入信号和输出信号;(b)~(d)图 3(a)中黑框处的局部放大图

Fig. 3 Simulation results for static/dynamic composite signal demodulation. (a) Input signals and output signals; (b)~(d) enlarged images of areas indicated by solid boxes in Fig. 3(a)

如图 3(b)所示,在腔长发生明显变化之前,两种不同的解调技术都很好地恢复出了待测信号。但是,对于对称解调技术来说,在腔长发生大幅度的改变之后,其计算得到的相位差与真实相位差出现了比较大的差别,因此导致了解调的失败,图 3(a)中信号 sym 的静态分量出现明显的错误。从图 3(c)也可以看出,在腔长发生较大幅度的改变之后,解调信号 sym 出现了明显的畸变。而改进对称解调技术在腔长出现较大幅度的改变后重新计算了此时的相位差,因此很好地恢复出待测信号。从图 3(a)和(d)可以看出,改进对称解调技术很好地解调出待测信号,腔长变化前后解调信号的动态分量都保持与输入信号一致,没有产生畸变。同时,从信号 c-sym 得到腔长的变化量为 70.38  $\mu\text{m}$ ,与输入的腔长变化量一致,误差约为 0.54%。

为了减少运算量,在腔长突变段,将腔长突变前后

相位差的均值作为突变段的相位差,在重新解调后利用相位差的变化反推腔长的变化量,从而对突变段进行校准。由于在突变段相位差变化大,因此使用固定的  $\delta$  进行解调时误差较大,在图 3 中可以明显看出,在腔长突变段,虽然经过校准,腔长的变化量保持准确,但解调信号 c-sym 逐渐偏离了 input。因此,如果关注待测信号的变化细节,可以对腔长突变段的相位差进行逐点计算,具体方法为:取该点前后一段时间内的原始信号,通过滑动计算获得突变段每个点对应的相位差,再进行待测信号解调;该方法的信号恢复精度高(如参考文献[23]中图 5 所示),但运算量很大。

### 4 实验与讨论

搭建如图 1 所示的解调仪。使用微调架构成腔长大幅度可调的 EFPI,同时可通过压电陶瓷(PZT)对其加载动态信号,以验证该解调方法对静态/动态复合信号的解调能力。实验前后传感器腔长的变化量由光谱域白光干涉测量仪(WLI)获得<sup>[13]</sup>。

使用信号发生器在传感器上加载 100 Hz 的正弦信号,实验中通过调整微调架改变 EFPI 的腔长以施加静态分量。实验前,通过 WLI 获得传感器的腔长为 218.09  $\mu\text{m}$ ;实验结束后,通过 WLI 得到传感器的腔长为 267.92  $\mu\text{m}$ 。实验前后腔长的变化量为 49.83  $\mu\text{m}$ 。通过该解调仪进行解调,实验数据如图 4 所示。图 4(a)为通过解调仪获得的静态/动态复合信号,图中信号 sym 为对称解调技术的解调信号,信号 c-sym 为改进对称解调技术的解调信号,图 4(b)~(e)分别为图 4(a)中黑框处的局部放大图。从图 4(a)可以获得 sym、c-sym 中腔长的变化量分别为 47.22  $\mu\text{m}$ 、50.86  $\mu\text{m}$ 。显然,由于腔长出现较大幅度的变化,对称解调技术出现明显的误差。从图 4(c)、(d)可以看出,由于相位差计算的错误,对称解调技术解调的信号动态分量出现明显畸变。改进对称解调技术则很好地恢复出待测信号,其直流分量的测量误差为 2.07%。从图 4(b)、(c)、(e)可以看出:腔长发生明显变化后,信号 c-sym 的动态分量保持一致,其峰峰值分别为 408.33 nm、407.58 nm、402.17 nm,其振幅的变化幅度为 1.53%,振幅差异主要来源于 PZT 性能限制。c-sym 动态分量的功率谱如图 5 所示,信号频率为 100 Hz,与输入信号一致。本实验证明该解调技术能够用来解调静态/动态复合信号。

改进对称解调技术可以在传感器的腔长变化量超过 100  $\mu\text{m}$  时正常解调出待测信号。同样地,在传感器上加载 100 Hz 的正弦信号,通过微调架大幅度改变 EFPI 的腔长。通过 WLI 获得实验前后传感器的腔长为 222.76  $\mu\text{m}$ 、326.80  $\mu\text{m}$ ,腔长的变化量为 104.04  $\mu\text{m}$ 。通过该解调仪进行解调,实验数据如图 6 所示。图 6(a)为通过解调仪获得的静态/动态复合信号,图 6(b)、(c)分别为图 6(a)中矩形框处的局部放大

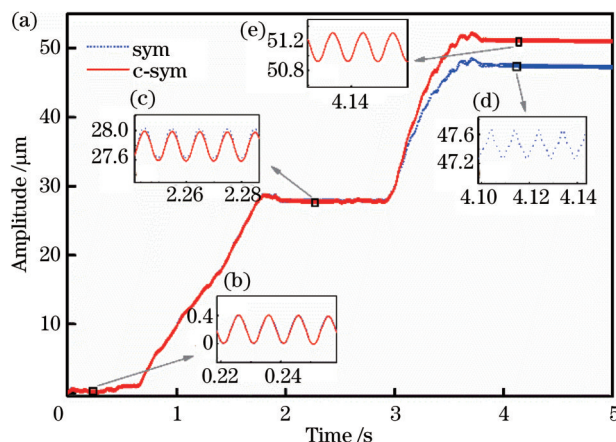


图4 静态/动态复合信号的解调结果。(a)解调得到的静态/动态复合信号;(b)~(e)图4(a)中黑框处的局部放大图

Fig. 4 Demodulation results of static/dynamic composite signals. (a) Recovered static/dynamic composite signals; (b)–(e) enlarged images of areas indicated by solid boxes in Fig. 4(a)

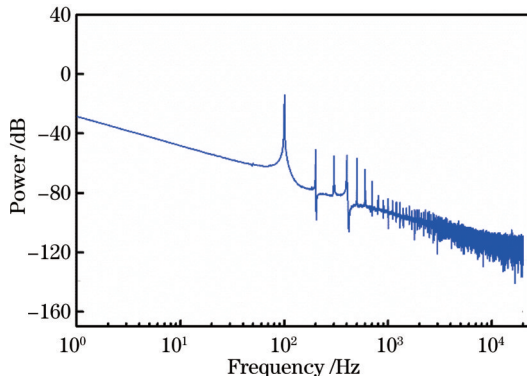


图5 信号c-sym中动态分量的功率谱

Fig. 5 Power spectrum of dynamic component of signal c-sym  
图。从图6可知,由解调信号所得的腔长变化量为 $106.38 \mu\text{m}$ ,与输入信号一致,误差约为2.25%。图6(b)、(c)中解调所得的动态分量保持一致,并无畸变的情况出现,二者的峰峰值分别为 $820.96 \text{ nm}$ 、 $815.74 \text{ nm}$ ,其振幅的变化幅度为0.64%,同样保持一致。通过本实验证明该技术在腔长变化 $100 \mu\text{m}$ 时仍然能够正常解调信号。图4及图6中信号动态分量的解调精度较高,但是该技术对大幅度腔长变化量的测量误差在2%附近,大于仿真的误差水平,其主要原因在于光源波长漂变造成信号间相位差并不完全相等,同时,微调架在调整后需要一定时间才能稳定,导致WLI测量的腔长与实验中的腔长存在差别。

改进对称解调技术的可测量动态信号的频率范围与三波长对称解调技术一致<sup>[23]</sup>,其在解调原理上并不存在对待测信号频率的限制。基于该技术的解调仪可测量动态信号的频率范围只受采集卡采样频率以及光电子管等电子器件带宽的限制,本文采用的采集卡的最高采样频率较低,为200 kHz,根据奈奎斯特采样定

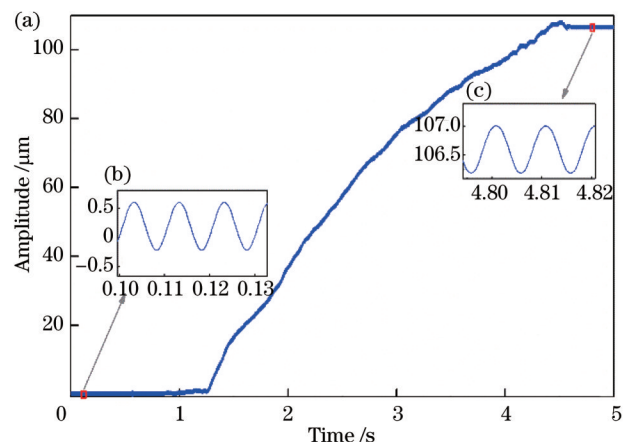


图6 腔长变化大于 $100 \mu\text{m}$ 时的静态/动态复合信号的解调结果。(a)解调得到的静态/动态复合信号;(b)(c)图6(a)中矩形框处的局部放大图

Fig. 6 Demodulation results for static/dynamic composite signal with cavity length change larger than  $100 \mu\text{m}$ . (a) Recovered static/dynamic composite signals; (b)(c) enlarged images of areas indicated by solid boxes in Fig. 6(a)

理,其所能解调的信号最高频率为100 kHz。

## 5 结 论

提出了一种可解调EFPI传感器静态/动态复合信号的改进对称解调技术。在对称解调技术的基础上,通过输出信号的直流量判断传感器腔长的变化,从而划分腔长稳定段与突变段,分段并重新进行信号解调,以保证动态分量的解调精度;同时利用腔长变化前后计算出的干涉信号相位差对腔长的变化量进行补偿,提高静态分量的测量精度。该技术在腔长大幅度变化的情况下也能够正常执行,能够实现对静态/动态复合信号的测量。而且该技术属于无源解调技术,适用于对高频信号进行解调。通过仿真与实验证明该方案能够实现对静态/动态复合信号的测量。实验中实现了幅度超过 $100 \mu\text{m}$ 复合信号的解调。该解调技术精度较高,对大幅度腔长变化量的测量误差约为2%。该解调技术具有系统简单、稳定、低成本、应用范围广等优势,具有较广阔的应用前景。

## 参 考 文 献

- [1] 廖延彪,苑立波,田芊.中国光纤传感40年[J].光学学报,2018,38(3): 0328001.  
Liao Y B, Yuan L B, Tian Q. The 40 years of optical fiber sensors in China[J]. Acta Optica Sinica, 2018, 38(3): 0328001.
- [2] 周超然,童杏林,靳其兵,等.面向石化生产的光纤传感技术进展[J].激光杂志,2022,43(8): 13-18.  
Zhou C R, Tong X L, Jin Q B, et al. Research progress of optical fiber sensing technology for high temperature environment of petrochemical production[J]. Laser Journal, 2022, 43(8): 13-18.
- [3] Zhao S X, Liu Q W, Ma H L, et al. White-light-driven resonant fiber-optic gyro based on round trip filtering scheme[J].

- Optics Letters, 2022, 47(5): 1137-1140.
- [4] Gong Y F, Shi J H, Guang D, et al. Improved algorithm for phase generation carrier to eliminate the influence of modulation depth with multi-harmonics frequency mixing[J]. Journal of Lightwave Technology, 2023, 41(5): 1357-1363.
- [5] 刘丹, 赵聪, 纪朋, 等. 基于光纤端面双光子聚合微柱的丙酮气体传感器[J]. 中国激光, 2022, 49(12): 1210002.
- Liu D, Zhao C, Ji P, et al. Acetone gas sensor based on optical fiber end-face two-photon polymerization microcolumn[J]. Chinese Journal of Lasers, 2022, 49(12): 1210002.
- [6] 江毅, 高红春, 贾景善. 光谱域光纤白光干涉测量技术[J]. 计测技术, 2018, 38(3): 31-42.
- Jiang Y, Gao H C, Jia J S. Fiber optical spectral-domain white-light interferometry[J]. Metrology & Measurement Technology, 2018, 38(3): 31-42.
- [7] 张树桓, 江毅. 非本征法布里-珀罗干涉型传感器非周期信号的相位解调方法[J]. 光学学报, 2022, 42(9): 0906002.
- Zhang S H, Jiang Y. Phase demodulation method for non-periodic signal in extrinsic Fabry-Perot interferometric sensor[J]. Acta Optica Sinica, 2022, 42(9): 0906002.
- [8] Liu Q, Li A, Liu Y Y, et al. TWDM-assisted active quadrature demodulation of fiber-optic Fabry-Perot acoustic sensor network [J]. Journal of Lightwave Technology, 2021, 39(12): 3991-3997.
- [9] Zhang W J, Lu P, Qu Z Y, et al. Four-wavelength quadrature phase demodulation technique for extrinsic Fabry-Perot interferometric sensors[J]. Optics Letters, 2022, 47(10): 2406-2409.
- [10] Liu Y, Qi B, Winder D E. Faraday Michelson interferometers for signal demodulation of fiber-optic sensors[J]. Journal of Lightwave Technology, 2021, 39(8): 2552-2558.
- [11] Huang Y, Wang S, Jiang J F, et al. Orthogonal phase demodulation of optical fiber Fabry-Perot interferometer based on birefringent crystals and polarization technology[J]. IEEE Photonics Journal, 2020, 12(3): 7101209.
- [12] 王东平, 王伟, 张军英, 等. 光纤法布里-珀罗传感器双峰-干涉级次定位联合解调算法[J]. 光学学报, 2022, 42(16): 1628001.
- Wang D P, Wang W, Zhang J Y, et al. Joint demodulation algorithm of bimodal-interference order positioning for optical fiber Fabry-Perot sensor[J]. Acta Optica Sinica, 2022, 42(16): 1628001.
- [13] Jiang Y. Fourier transform white-light interferometry for the measurement of fiber-optic extrinsic Fabry-Pérot interferometric sensors[J]. IEEE Photonics Technology Letters, 2008, 20(2): 75-77.
- [14] Yu Z H, Wang A B. Fast demodulation algorithm for multiplexed low-finesse Fabry-Pérot interferometers[J]. Journal of Lightwave Technology, 2016, 34(3): 1015-1019.
- [15] Liu W, Yang T Y, Shi Y J, et al. White light interference demodulation of optical fiber Fabry-Perot micro-pressure sensors based on the Karhunen-Loeve transform and singular value decomposition[J]. Optics Express, 2022, 30(4): 5618-5633.
- [16] Liu Q, Li S M, Zhou D P, et al. Compressed-sensing fiber-optic white light interferometry[J]. Optics Letters, 2021, 46(19): 4944-4947.
- [17] Ferreira M S, Bierlich J, Kobelke J, et al. Negative curvature hollow core fiber sensor for the measurement of strain and temperature[J]. Optics Express, 2021, 29(4): 5808-5818.
- [18] Tian K, Zhang M Y, Zhao Z Y, et al. Ultra-compact in-core-parallel-written FBG and Mach-Zehnder interferometer for simultaneous measurement of strain and temperature[J]. Optics Letters, 2021, 46(22): 5595-5598.
- [19] Liu Q, Jing Z G, Li A, et al. Simultaneous measurement of vibration and temperature using frequency-scanned parallel phase-shifting interferometry[J]. Journal of Lightwave Technology, 2021, 39(12): 4094-4100.
- [20] Chen J M, Xue C Y, Zheng Y Q, et al. Micro-fiber-optic acoustic sensor based on high-Q resonance effect using Fabry-Pérot etalon[J]. Optics Express, 2021, 29(11): 16447-16454.
- [21] Liao H, Lu P, Liu L, et al. Phase demodulation of short-cavity Fabry-Perot interferometric acoustic sensors with two wavelengths[J]. IEEE Photonics Journal, 2017, 9(2): 7102207.
- [22] Ren Q Y, Jia P G, An G W, et al. Self-compensation three-wavelength demodulation method for the large phase extraction of extrinsic Fabry-Pérot interferometric sensors[J]. Optics and Lasers in Engineering, 2023, 164: 107535.
- [23] Jia J S, Jiang Y, Huang J B, et al. Symmetrical demodulation method for the phase recovery of extrinsic Fabry-Perot interferometric sensors[J]. Optics Express, 2020, 28(7): 9149-9157.

## Corrected Symmetrical Demodulation Method for Static/Dynamic Composite Signals

Jia Jingshan\*

College of Communication and Information Technology, Xi'an University of Science and Technology, Xi'an  
710054, Shaanxi, China

### Abstract

**Objective** Extrinsic Fabry-Perot interferometers (EFPIs) are widely used in fiber optic sensors. In many applications, the measurand is a mixture of static and dynamic signals. However, laser interference demodulation algorithms used for dynamic signal measurement are significantly different from white light interference demodulation algorithms used for static signal measurement. Laser interference demodulation algorithms require laser wavelengths to remain stable, while white light interference demodulation algorithms require wavelength scanning to obtain the spectrum of the sensor to achieve measurement. Therefore, these measurement techniques can only measure different dynamic signals or different static signals and cannot achieve measurement of static/dynamic composite signals. For EFPI sensors, it is expected to achieve the measurement of static/dynamic composite signals through high-speed white light interferometry demodulation

technologies. However, these demodulation technologies are still unable to meet the measurement requirements of high-frequency signals due to limitations in scanning speed. Some high-speed white light interferometry demodulation technologies rely on high-tuning-speed laser sources, but the bandwidth of such light sources is narrow, which limits the measurement range. At the same time, this type of technology requires a large amount of calculations and sometimes requires offline signal processing. Various laser interference demodulation algorithms have been proposed to extract dynamic signals from EFPI sensors. However, these demodulation techniques will collapse if the EFPI cavity length changes significantly since the cavity length and laser wavelengths must be strictly matched to obtain orthogonal signals. In this article, a correction symmetrical demodulation method for the measurement of static/dynamic composite signals is proposed. Static/dynamic composite signal demodulation is experimentally demonstrated.

**Methods** The change in sensor cavity length is judged by the direct current component of the output signal of the symmetrical demodulation method. Then, the output signal is divided into stable segments and abrupt segments. The measurand is then re-demodulated segment by segment to improve the demodulation accuracy of the dynamic component. Phase differences calculated before and after the abrupt segment are used to compensate for the change in cavity length, and the demodulation accuracy of static components is improved. The process of static/dynamic composite signal demodulation is as follows: 1) the preliminary demodulation signal  $d_t$  is recovered through Eq. (11). 2) the signal  $d_t$  is divided into stable segments and abrupt segments. 3) the phase difference  $\delta$  for each stable segment is calculated. 4) the average value of  $\delta$  before and after the abrupt segment is used as the phase difference of the abrupt segment to re-demodulate the signal. Eq. (4) is then used to calculate cavity lengths before and after the abrupt segment, and the cavity length change of the abrupt segment is calibrated. 5) the measurand of each stable segment is re-demodulated and combined with the calibrated abrupt segment demodulation signals to obtain the complete output signal  $d_s$ .

**Results and Discussions** Static/dynamic composite signals can be demodulated by the proposed demodulation method, which is experimentally demonstrated, as shown in Fig. 4. The cavity length change of the c-sym in Fig. 4(a) is  $50.86 \mu\text{m}$ , which is consistent with the cavity length change measured by the white light interference demodulation algorithm. The measurement error of the static component is 2.07%. Figures 4(b)–(e) show that the dynamic component of the c-sym remains consistent despite the cavity length changes significantly. The peak-to-peak amplitudes are 408.33 nm, 407.58 nm, and 402.17 nm. The amplitude variation is 1.53%. The power spectrum of the dynamic component of the c-sym is plotted in Fig. 5. The frequency is 100 Hz, which is consistent with the frequency of the input signal. The proposed demodulation method can be performed normally even if the cavity length changes up to  $100 \mu\text{m}$ , as shown in Fig. 6. The frequency range of the proposed demodulation method is consistent with that of the symmetrical demodulation method and is not limited by the demodulation principle. The frequency range of the demodulator is only limited by the sampling frequency of the analog-to-digital converter and the bandwidth of electronic devices such as photodiodes. The analog-to-digital converter of the demodulator has a sampling frequency of 200 kHz. According to the Nyquist sampling theorem, the maximum frequency of the signal which the demodulator can demodulate is 100 kHz.

**Conclusions** In conclusion, a correction symmetrical demodulation method for the measurement of static/dynamic composite signals is proposed. The demodulation capability of the demodulator to static/dynamic composite signals is experimentally investigated. The measurement of a cavity length change with an amplitude of  $100 \mu\text{m}$  is achieved. The measurement error is about 2% for large changes in cavity length. The technique is applicable to static/dynamic composite signals applied on sensors with different cavity lengths.

**Key words** fiber optics; fiber sensing technique; laser interferometry; phase demodulation; extrinsic Fabry-Perot interferometer